Available online www.jocpr.com

Journal of Chemical and Pharmaceutical Research, 2016, 8(8):892-898

Research Article

ISSN : 0975-7384
CODEN(USA) : JCPRC5

Study of physico-chemical, structural, thermal and in-vitro characteristics of zinc and magnesium substituted nanodimensional hydroxyapatite

Seema Kapoor[a*], Uma Batra[b], Sonia Sharma[a] and Suchita Kohli[a]

[a]*Dr. SSB University Institute of Chemical Engineering & Technology, Panjab University, Chandigarh, India*
[b]*Dept. of Materials & Metallurgical Engineering, PEC University of Technology, Chandigarh, India*

ABSTRACT

Hydroxyapatite (HA) is one of the most important calcium phosphates for hard tissue replacement in human bodies. Recently, cation substituted HA has been a research focus in order to enhance HA bioactivity and to adapt various application requirements. The study was aimed at investigating the contribution of zinc (Zn) and magnesium (Mg) ions when substituted into the structure of HA. The substituted samples were synthesized through a sol-gel route and then calcined at 800°C, 1000°C and 1200°C. Comprehensive characterization techniques, including transmission electron microscopy, BET surface area, X-ray diffraction, Fourier transform infrared spectroscopy, thermogravimetric and in-vitro analysis provided experimental evidence of the effects of ion substitution on the morphology, crystallite size, BET surface area, phase transformations, crystallinity, functional groups, thermal stability and bioactive behavior of HA. The results showed that as-synthesized zinc substituted hydroxyapatite (ZnHA) and magnesium substituted hydroxyapatite (MgHA) nanopowders consisted of flake-like agglomerates and the length of particles varied in the range 26-36 nm and 15-19 nm, respectively. The thermal stability and surface area was higher for ZnHA than MgHA nanopowder. In-vitro analysis of nanopowders on immersion in simulated body fluid (SBF) showed trend of alternate decrease and increase in pH of SBF confirming the bioactive behavior of nanopowders.

Keywords: Nanodimensional, sol-gel, hydroxyapatite, zinc, magnesium, in-vitro, *β*-tricalcium phosphate

INTRODUCTION

Calcium phosphates (Ca-P) have been considered as useful materials for bone repair and replacement. Their involvement in mineralization processes is attributed to their versatility in accepting a large variety of substitution ions. Hydroxyapatite has been widely used to repair damaged or diseased hard tissues owing to its biocompatible, bioactive and osteoconductive nature [1, 2]. Various ions like cations (Zn^{2+}, Mg^{2+}, Mn^{2+}, Sr^{2+}, Na^{+}, K^{+}) or anions (F^{-}, Cl^{-}, HPO_4^{2-}, SiO_4^{4-} or CO_3^{2-}) [3, 4] are present in biological apatites. By ionic substitution in synthetic HA, properties like bioactivity and biocompatibility can be significantly improved [5]. Magnesium and zinc are potentially important trace ions in human hard tissues and they partially substitute for calcium in the HA structure.
Zinc (Zn) is capable of increasing osteoblast proliferation, biomineralization and bone formation. Its incorporation modulates morphology and crystallinity of biological apatite crystals. It is one of the most effective metal ions which inhibit crystal growth [6-9]. Magnesium (Mg) plays an important role in bone growth, since it affects osteoblast and osteoclast activity [10]. It offers inhibitory effect on HA nucleation and growth [11]. Mg incorporation in HA showed increased solubility with respect to stoichiometric HA [12] and reduced degree of crystallinity and the lattice parameters. In order to study the influence of Zn and Mg substitution in HA, this work presents a systematic and complete investigation of ZnHA and MgHA nanopowders synthesized via sol-gel route.

EXPERIMENTAL SECTION

Synthesis of nanopowders

Nanodimensional ZnHA and MgHA powders were synthesized via sol-gel route using calcium nitrate tetrahydrate (CNT, $Ca(NO_3)_2.4H_2O$, Merck, AR grade), zinc nitrate tetrahydrate (ZNT, $Zn(NO_3)_2.4H_2O$, Merck, AR grade), magnesium nitrate tetrahydrate (MNT, $MgNO_3.6H_2O$ Merck, AR grade) and potassium dihydrogen phosphate (KDP, KH_2PO_4, Merck, AR grade) as precursors of calcium, zinc, magnesium and phosphorous, respectively. For the synthesis of ZnHA nanopowder, 0.02 M ZNT was added to 0.98 M CNT solution (Solution A) and for MgHA nanopowder, 0.02 M MNT was added to 0.98 M CNT solution (Solution B). The solutions of precursors were prepared in double distilled water (DDW). The molar ratios (Ca+Zn)/P and (Ca+Mg)/P of as-synthesized ZnHA and MgHA nanopowders were maintained at 1.67. ZnHA nanopowder was obtained by adding dropwise (3-4 drops) 1.0 M aqueous Solution A to 0.6 M KDP solution and MgHA nanopowder was obtained by adding dropwise (3-4 drops) 1.0 M aqueous Solution B to 0.6 M KDP solution, under continuous stirring at 1000 rpm for 1 hour at room temperature. The pH was continuously monitored and adjusted to 10 ± 0.1 by adding 25% ammonium hydroxide (NH_4OH, Merck, India) solution to improve gelation and polymerization of HA structure. Gels obtained were aged at room temperature for 24 hours. Gelatinous precipitates formed were filtered by a centrifuge and washed thoroughly by lukewarm DDW. The precipitates were dried in an oven at 70°C for 24 hours and the powders were prepared by crushing the dried gels.

The as-synthesized ZnHA and MgHA nanopowders were calcined in a programmable type silicon carbide muffle furnace at 10°C/min in the temperature range of 800-1200°C. ZnHA samples calcined at 800°C, 1000°C and 1200°C were designated as ZnHA8, ZnHA10 and ZnHA12; MgHA samples calcined at 800°C, 1000°C and 1200°C were designated as MgHA8, MgHA10, and MgHA12, respectively.

Characterization of nanopowders

Transmission Electron Microscope (TEM) was used to assess the morphology and size of nanopowders using Hitachi, 7500 with resolution of 0.2 nm, operated at an accelerating voltage of 80-100 KV.

The BET surface area of powders was determined using Quantachrome Instruments NOVA 2200e Surface Area Analyser using Brunauer–Emmett–Teller (BET) method [13]. The linearized form of BET equation is expressed by:

$$\frac{p}{v(p_o - p)} = \frac{1}{v_m z} + \frac{z-1}{v_m z}\frac{p}{p_o} \qquad (1)$$

where p/p_0 is the relative vapour pressure of the adsorbate, v is the volume of gas adsorbed, v_m is the volume of gas adsorbed in a monolayer and z is a constant related to the energy of adsorption. The minimum relative pressure p/p_0 resolution was 2×10^{-5}. A linear regression of the left side of BET equation and p/p_0 yields a slope and intercept from which z and v_m are obtained. The BET surface area is then calculated from v_m [14].

X-ray diffraction (XRD, Philips X'Pert 1710) analysis using Cu K_α radiation, $\lambda = 1.54$ Å, 2θ- 20˚ to 80˚, step size 0.017°, time per step 20.03 s and scan speed 0.005 °/s was used for phase structure analysis. External standard method was used for determining relative amount of different phases present in nanopowders. Both cell parameters, a and c were calculated using the equation given below [15]:

$$\frac{1}{d^2} = 4/3 \left[\frac{h^2 + hk + k^2}{a^2} \right] + \frac{l^2}{c^2} \qquad (2)$$

where d is the distance between adjacent planes in the set of Miller indices (h k l), the reference for HA being JCPDS file no. 09-0432 (a = 9.418 Å, b = 9.418 Å, c = 6.884 Å, space group *p63/m*) and for β-tricalcium phosphate (β-TCP) being JCPDS file no. 09-0169 (a = 10.432 Å,b = 10.432 Å, c = 37.39 Å, space group *R*3*c* (167)). Crystallite size of nanopowders was calculated using Scherrer's equation [16, 17]:

$$X_s = \frac{0.9\lambda}{\beta \cos \theta} \qquad (3)$$

where X_S is the crystallite size in nm, λ is the wave length of X-ray beam, β is the broadening of diffraction line at half of its maximum intensity in radians and θ is the Bragg's diffraction angle (^{o}). The crystallinity degree (Xc) of nanopowders was evaluated as follows:

$$X_c = 1 - V_{112/300} / I_{300} \quad (4)$$

where I_{300} is the intensity of (3 0 0) reflection of HA and $V_{112/300}$ is the intensity of the hollow between (1 1 2) and (3 0 0) reflections, which completely disappears in non-crystallline samples. In agreement with Landi et al. [18], verification was made as follows:

$$\beta_{002} \; 3\sqrt{X_c} = K \quad (5)$$

where K is a constant equal to 0.24 for a very large number of different hydroxyapatite powders and β_{002} is the full width of the peak at half intensity of (0 0 2) reflection in degree 2θ.

Fourier transform infrared spectroscopy (FTIR Perkin Elmer) in the range of 400–4000 cm^{-1} using KBr pellets (1% wt/wt), with spectral resolution of 2 cm^{-1} was used to analyze the functional groups.

Simultaneous thermogravimetry and differential thermal analysis (TG/DTA, Perkin Elmer STA 6000), with an accuracy of ± 0.1 µg in weight measurement and ± 0.5 °C in temperature measurement was used to analyse the thermal behavior. All the tests were performed in air environment at heating rate 10 °C/min and air flow 20.0 ml/min.

The bioactivity evaluation of nanopowders was performed in simulated body fluid (SBF). The nanopowders were immersed individually in SBF (pH=7.24) in polystyrene bottles and were placed in a biological incubator at 37°C for 30 days.

RESULTS AND DISCUSSION

Microstructure and BET surface area of ZnHA and MgHA nanopowders

TEM micrographs of as-synthesized and calcined ZnHA and MgHA nanopowders are shown in Fig. 1. Both ZnHA and MgHA nanopowders exhibited flake-like morphology, which is in good agreement with literature [19, 20]. The length of these flakes varied in the range 26-36 nm and 15-19 nm for ZnHA and MgHA nanopowders, respectively.
The TEM results revealed the morphological changes in calcined nanopowders. It was observed that on calcination, both ZnHA and MgHA nanopowders underwent agglomeration. It has been reported in literature that the high surface energy of nanoparticles results in agglomeration [21]. ZnHA and MgHA nanopowders calcined at 800°C exhibited catenulate morphology and particle coarsening with mean crystallite sizes of 41 nm and 38 nm, respectively. Calcination at 1000°C and 1200°C induced remarkable grain coarsening. According to Yoshida et al. [22], the presence of divalent substitution of cations induces enhancement in HA sinterability.

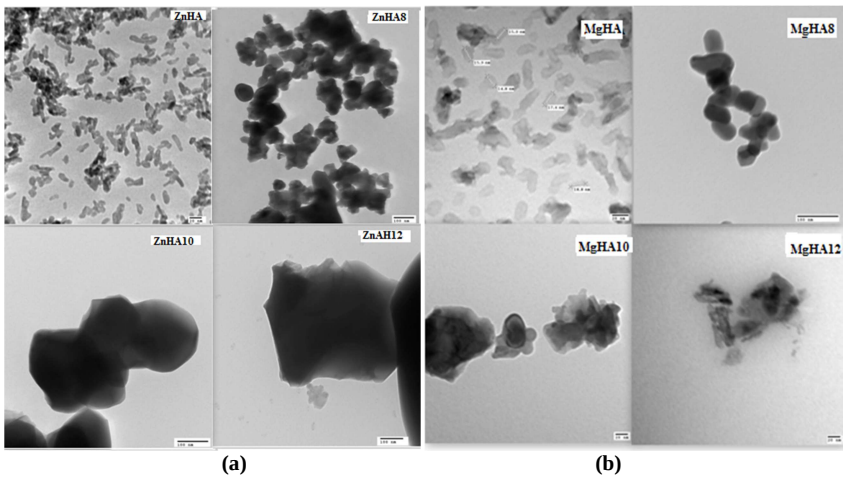

Fig. 1 TEM micrographs of as-synthesized and calcined (a) ZnHA (b) MgHA nanopowders

Phase analysis, crystallinity and crystallite size of ZnHA and MgHA nanopowders

XRD spectra of as-synthesized ZnHA and MgHA nanopowders (Fig. 2) revealed the presence of hydroxyapatite and calcium deficient hydroxyapatite (CDHA). The nanopowders were amorphous in nature, which is in good agreement with literature [24, 25]. The nanopowders evidenced merged reflections in the 2θ range of 28-32° and 45-55° [25].

This suggested the increased reticular defects in apatite lattice and partial substitution of Zn^{2+} and Mg^{2+} ion for Ca^{2+} ion [12].

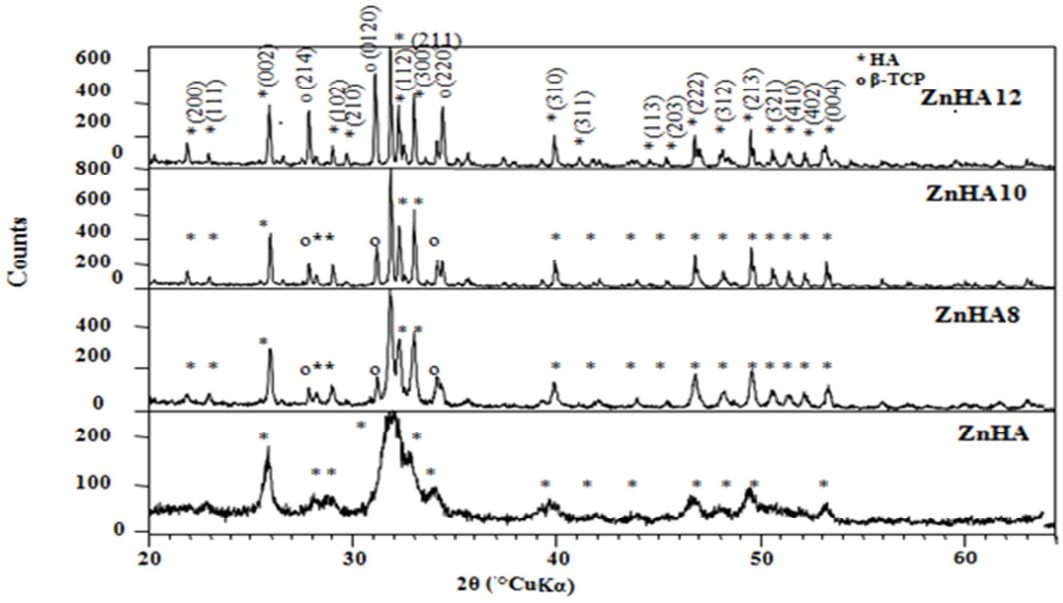

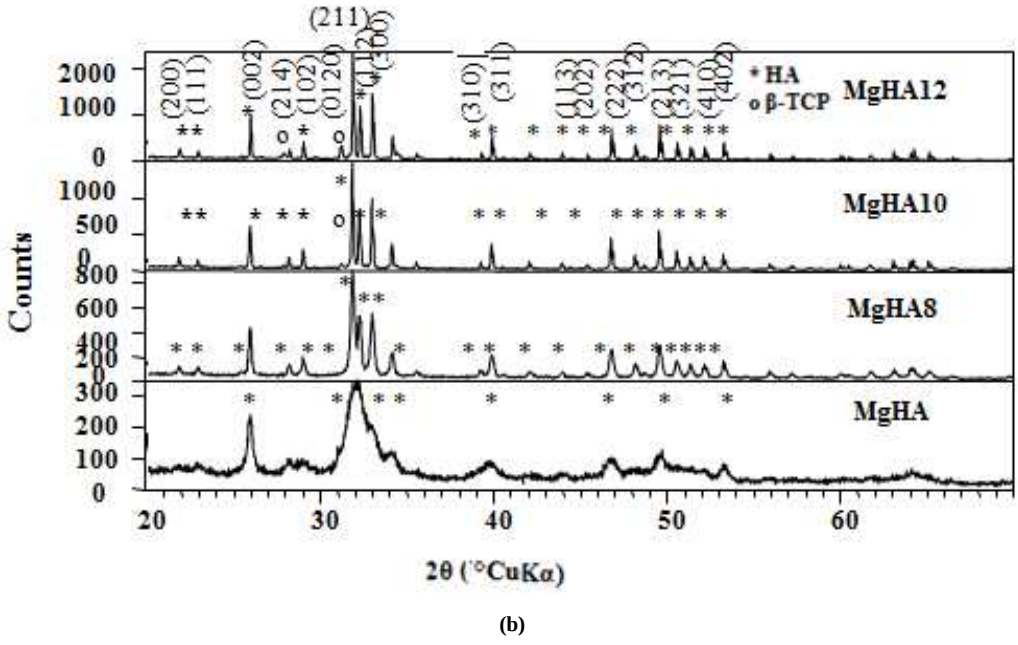

Fig. 2 XRD patterns of as-synthesized and calcined (a) ZnHA (b) MgHA nanopowders

The mean crystallite size and lattice parameters of ZnHA nanopowders were higher than MgHA nanopowders (Table 1), which might be due to larger ionic radius of Zn^{2+} (0.75 Å) with respect to Mg^{2+} (0.65 Å) [26, 27]. Table 2 reports the peak width measurement of (0 0 2) and (3 1 0) reflections and crystallinity of ZnHA and MgHA nanopowders. Higher broadening of the peaks for (0 0 2) and (3 1 0) reflections in MgHA nanopowder than in ZnHA nanopowder indicates lower crystallinity of former than latter.

Table 1 Calculated structural parameters of as-synthesized ZnHA and MgHA nanopowders

Sample	Mean crystallite size (nm)	Lattice parameters			
		a=*b* (Å)	*c* (Å)	*c*/*a* ratio	$V=3a^2c$ [Å]^3
ZnHA	29	9.451	6.895	0.7310	1847.61
MgHA	17	9.390	6.860	0.7300	1815.00
HA (JCPDS file no. 09-0432)	-	9.418	6.884	0.7309	1831.00
CDHA (JCPDS file no. 46-0905)	-	9.441	6.881	0.7288	1839.96

Table 2 Peak width measurement of (0 0 2) and (3 1 0) reflections and crystallinity of ZnHA and MgHA nanopowders

	Planes	ZnHA	MgHA
Peak width (2θ)	(0 0 2)	0.2342	0.3361
	(3 1 0)	0.2686	0.7656
Crystallinity		0.12	0.11

As reported by Fathi et al. [28], calcium deficient hydroxyapatite (CDHA) changes to stoichiometric HA and β-TCP on calcination, according to the following Eq.:

$$Ca_{10-x}(HPO_4)_x(PO_4)_{6-x}(OH)_{2-x} \rightarrow (1\text{-}x)Ca_{10}(PO_4)_6(OH)_2 + 3x\beta\text{-}Ca_3(PO_4)_2 + x\ H_2O \qquad (6)$$

where x is the calcium deficiency. On calcination, the degree of decomposition was estimated from XRD patterns of calcined ZnHA and MgHA nanopowders, in terms of the molar ratio of HA and β-TCP phase in biphasic mixture [29]. From XRD patterns using external standard method, the estimated weight fractions of HA (W_{HA}) and β-TCP ($W_{\beta\text{-TCP}}$) were converted into mole fractions and then used for calculating x and Ca/P values [29]. The molar ratio of β-TCP to HA is given by $3x/1\text{-}x$ in calcined powders and Ca/P molar ratio is equal to $(10\text{-}x)/6$ [30]. W_{HA}, $W_{\beta\text{-TCP}}$ and Ca/P molar ratios for calcined ZnHA and MgHA nanopowders are compared in Table 3. $W_{\beta\text{-TCP}}$ was higher in MgHA10 and MgHA12 than ZnHA10 and ZnHA12 nanopowders, indicating that MgHA nanopowders were thermally less stable than ZnHA nanopowders i.e. the substitution of Mg in apatite promoted formation of β-TCP.

Table 3 Weight fractions of HA & β-TCP phases and Ca/P molar ratio in calcined ZnHA and MgHA nanopowders

	Phase	ZnHA10	ZnHA12	MgHA10	MgHA12
Constituent weight fraction	W_{HA}	0.68	0.51	0.42	0.35
	$W_{\beta\text{-TCP}}$	0.32	0.49	0.58	0.65
Estimated Ca/P molar ratio		1.61	1.58	1.57	1.56

The mean crystallite sizes of ZnHA and MgHA nanopowders increased with increase in calcination temperature till 1000°C, which might be due to the agglomeration and sintering effect in particles during calcination (Table 4). Nanopowders calcined at 1200°C showed lower mean crystallite size than nanopowders calcined at 1000°C, which probably was due to decomposition of HA phase to β-TCP at temperatures above 1000˚C. It was observed that crystallinity of nanopowders increased with increase in calcination temperature.

Table 4 Mean crystallite sizes and crystallinity of calcined ZnHA and MgHA nanopowders

Sample	ZnHA8	ZnHA10	ZnHA12	MgHA8	MgHA10	MgHA12
Mean crystallite size, nm	41	74	62	38	127	92
Crystallinity (X_c)	0.74	0.91	0.92	0.76	0.93	0.95

FTIR analysis of ZnHA and MgHA nanopowders

FTIR spectra of ZnHA and MgHA nanopowders are reported in Fig. 3. Both nanopowders showed the characteristic pattern of hydroxyapatite [31]: hydroxyl vibrations at ν OH (3567 cm^{-1}) and δ OH (633 cm^{-1}); phosphate vibrations at ν_1 PO_4 (962 cm^{-1}), ν_3 PO_4 (broad band 1033-1094 cm^{-1}) and ν_4 PO_4 (565 cm^{-1} and 603 cm^{-1}). The peaks of hydroxyl groups and phosphate groups showed remarkable decrease in calcined nanopowders [32].

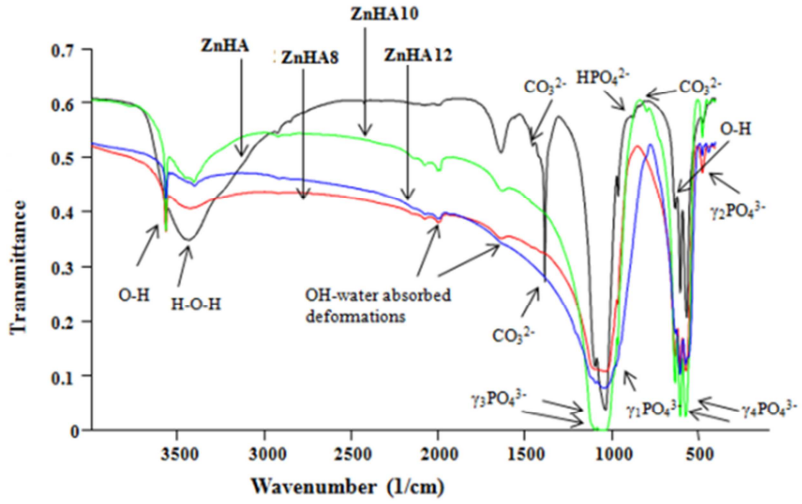

(a)

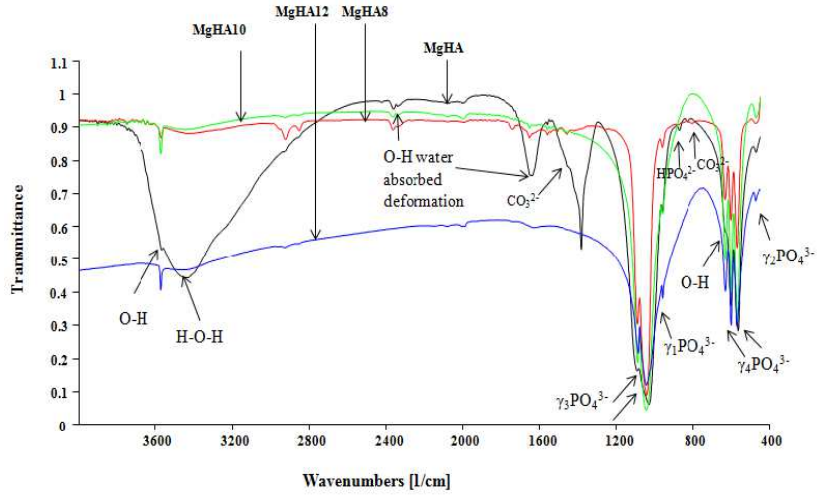

(b)

Fig. 3 FTIR Spectra of as-synthesized and calcined (a) ZnHA (b) MgHA nanopowders

Thermal behaviour of ZnHA and MgHA nanopowders

The TGA of ZnHA and MgHA nanopowders showed that the thermal stability of ZnHA was higher than MgHA, with weight loss of 10.39% from room temperature to 1000°C against 45% for MgHA. ZnHA nanopowder showed weight loss in three temperature regions: 25-300°C (5.9%), 300-600°C (2.84%) and 600-1000°C (1.65%), whereas MgHA showed weight loss in two regions: 25-700°C (33%) and 700-1000°C (12%). The weight loss below 300°C was due to desorption of water from the surface of the apatite. Between 300-600°C, conversion of HPO_4^{2-} ions of CDHA into $P_2O_7^{4-}$ ions occurred according to mechanism proposed by Mortier et al. [33]:

$$2HPO_4^{2-} \rightarrow P_2O_7^{4-} + H_2O \quad (7)$$

Above 600°C, weight loss was attributed to the reaction of OH^- ions of apatite and $P_2O_7^{4-}$ ions formed at lower temperatures, with consequent loss of water as represented by following equation:

$$P_2O_7^{4-} + 2OH^- \rightarrow 2PO_4^{3-} + H_2O \quad (8)$$

The lesser weight loss in ZnHA (1.65%) than MgHA (12%) above 700°C indicated that the former has higher thermal stability. Also from XRD results, it was found that more wt.% of β-TCP phase formed in MgHA than ZnHA on calcination at 1000°C and 1200°C.

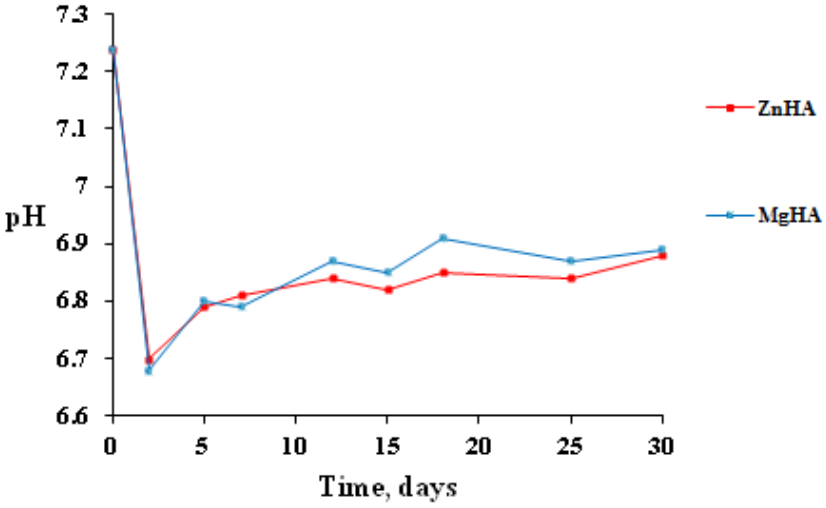

Fig. 4 pH change in SBF with time of immersion for as-synthesized ZnHA and MgHA nanopowders

***In-vitro* behaviour of ZnHA and MgHA nanopowders**

Fig. 4 shows the variation of pH values as a function of immersion time for as-synthesized ZnHA and MgHA nanopowders in SBF solution under the physiological conditions at 37°C up to 30 days. In-vitro analysis of both nanopowders showed almost similar trend of alternate decrease and increase in pH of SBF confirming the bioactive behavior of nanopowders.

CONCLUSION

Nanodimensional ZnHA and MgHA powders were successfully synthesized via a sol-gel route. They consisted of flake-like agglomerates with mean crystallite sizes of 29 nm and 17 nm, respectively. Calcium deficient hydroxyapatite phase of as-synthesized nanopowders transformed to biphasic mixture of HA and β-TCP on calcination. The surface area and thermal stability of ZnHA was higher than MgHA. In-vitro analysis showed bioactive behavior of both nanopowders. The same is expected under in-vivo conditions and is likely to help in promoting bone growth. Thus ceramics designed from hydroxyapatite containing Zn and Mg would be more suitable for dental and orthopedic applications.

Acknowledgments

This research was funded by Dr. SSBUICET, Panjab University, Chandigarh and PEC University of Technology, Chandigarh under Technical Education Quality Improvement Programme (TEQIP-II). One of the authors (Seema Kapoor) greatly acknowledges the financial support received under UGC Major Research Project, Government of India (F.No.-43-155/2014 (SR)).

REFERENCES

[1] LL Hench. *J. Am. Ceram. Soc.*, **1991**, 74, 1487-1510.
[2] H Arami; M Mohajerani; M Mazloumi; R Khalifehzadeh; A Lak; SK Sadrnezhaad. *J. Alloys Compd.*, **2009**, 469(1), 391-394.
[3] M Descamps; JC Hornez; A Leriche. *J. Eur.Ceram.Soc.*, **2009**, 2, 369-375.
[4] JC Elliott. Structure and chemistry of the apatites and other calcium orthophosphates. Elsevier, Amsterdam, **1994**.
[5] K Matsunaga; H Murata; T Mizoguchi; A Nakahira. *Acta Biomater.*, **2010**, 6, 2289-2293.
[6] MH Santos; P Valerio; AM Goes; MF Leite; LGD Henein. *Biomed. Mater.*, **2007**, 2, 135-141.
[7] N Kanzaki; K Onuma; G Treboux; S Tsutsumi; A. Ito. *J. Phys.Chem.B*, **2000**, 104,4189-4194.
[8] SJ Kalita; HA Bhatt. *Mater. Sci. Eng. C*, **2007**, 27, 37-848.
[9] L Ming'Ou; X Xiufeng; L Rongfang; C Cuiyu; H Lizhong. *J. Mater. Sci. Mater. Med.*, **2008**, 19, 797-803.
[10] M Percival. *Appl. Nutr. Sci. Reports*, **1999**, 5, 1-5.
[11] PN Kumta; C Sfeir; DH Lee; D Olton; D Choi. *Acta Biomater.*, **2005**, 1, 65-83.
[12] E Landi; G Logroscino; L Proietti; A Tampieri; M Sandri; S Sprio. *J. Mater. Sci. Mater. Med.*, **2008**, 19, 239-247.
[13] R Joseph; KE Tanner. *Biomacromolecules*, **2005**, 2(6), 1021-1026.
[14] L Clausen; I Fabricius. *J. Colloid Interface Sci.*, **2000**, 227, 7-15.
[15] TJ Webster; EA Massa-Schlueter; JL Smith; EB Slamovich. *Biomaterials*, **2004**, 25, 2111-2121.
[16] MH Fathi; A Hanifi; V Mortazavi. *J. Mater. Process. Tech.*, **2008**, 202, 536-542.
[17] R Jenkins; RL Snyder. Introduction to X-ray Powder Diffractometry. John Wiley and Sons, New York, **1996**.
[18] E Landi; A Tampieri; G Celottia; S Sprio. *J. Eur. Ceram. Soc.*, **2000**, 20, 2377-2387.
[19] D Norhidayu; I. Sopyan; S Ramesh. *Int. Conf. Construct. Buildg. Tech.*, **2008**, 24, 257-270.
[20] M Kheradmandfard; M Fathi. *J. Alloys Compd.*, **2010**, 504, 141-145.
[21] J Gomez-Morales; J Torrent-Burgues; R Rodriguez-Clemente. *Cryst Res. Technol.*, **2001**, 36, 1065-1074.
[22] K Yoshida; WN Kondo; H Kita. *J. Am. Ceram. Soc.*, **2005**, 88, 2315-2318.
[23] J Marchi; ACS Dantas; P Greil; JC Bressiani; AHA Bressiani; FA Muller. *Mater. Res. Bull.*, **2007**, 42, 1040-1050.
[24] WL Suchanek; K Byrappa; P Shuk; RE Riman; VF Janas; KS TenHuisen. *Biomaterials*, **2004**, 25, 4647-4657.
[25] A Bigi; G Falini; E Foresti; M Gazzano; A Ripamonti; N Roveri. *J. Inorg. Biochem.*, **1993**, 49, 69-75.
[26] F Miyaji; Y Kono; Y Suyama. *Mater. Res. Bull.*, **2005**, 40, 209-220.
[27] A Bigi; G Falini; E Foresti; M Gazzano; A Ripamonti; N Roveri. A*cta Crystallogr.*, **1996**, B52, 87-92.
[28] MH Fathi; A Hanifi. *Mater. Lett.*, **2007**, 61, 3978-3983.
[29] BD Cullity; SR Stock. Elements of X-Ray Diffraction, 3rd Edition, Prentice-Hall Inc., **2001**.
[30] S Raynaud; E Champion; D Bernache-Assollant; P Thomas. *Biomaterials*, **2002**, 23, 1065-1072.
[31] S Kannan; JMF Ferreira. *Chem. Mater.*, **2006**, 18, 198-203.
[32] IV Fadeev; LI Shvorneva; SM Barinov; VP Orlovskii. *Inorg. Mater.*, **2003**, 39, 947-950.
[33] A Mortie; J Lemaitre; PG Rouxhet. *Thermochim. Acta*, **1989**, 143, 265-282.